




# Rotating oil droplets driven by motile bacteria at interfaces†

Narendra K. Dewangan and Jacinta C. Conrad \*

Cite this: *Soft Matter*, 2019, 15, 9368

Received 5th August 2019,  
Accepted 30th October 2019

DOI: 10.1039/c9sm01570a

rsc.li/soft-matter-journal

We show that oil droplets suspended near a liquid–solid interface can be driven to rotate by motile bacteria adhered to the droplet surface. Droplets rotate clockwise when viewed from the liquid side, due to symmetry-breaking hydrodynamic interactions of bacteria with the interface. The angular speed of rotation for droplets decreases as their size is increased. Differences in the speed of rotation driven by *Escherichia coli*, *Shewanella haliotis*, and *Halomonas titanicae* bacteria reflects differences in the number of bacteria adhered at the droplet surface and their interfacial affinity. Adding surfactant reduces the number of adherent bacteria and hence lowers the speed of rotation. Together, these results demonstrate that bacterial activity can be used to manipulate suspended droplets.

## 1 Introduction

Active fluids<sup>1</sup> that contain biological motors<sup>2–5</sup> offer an intriguing route to actuation on the microscale. As one example, bacteria convert chemical energy into mechanical energy.<sup>6</sup> Numerous and diverse in species, they are inexpensive biological power sources. Using bacteria to rotate microscopic gears, as mixers or propellers,<sup>7</sup> or transport particles, for drug delivery,<sup>8–10</sup> requires fundamental understanding of how bacterial motility couples to object motion.

Small numbers of adherent bacteria can rotate and/or translate solid objects of size of order 10–100  $\mu\text{m}$ , up to one hundred times greater than their body dimensions and up to one million times greater in mass.<sup>11–19</sup> The speed and persistence of motion in such systems, however, are often limited by the lack of coherence in the orientation of cells and their flagella.<sup>11,13</sup> These limitations can be overcome by coupling the motion of collectively moving bacteria to asymmetric rotors, which break symmetry to provide a consistent direction of rotation.<sup>20–23</sup> Swimming *Escherichia coli* bacteria at concentrations of order  $10^{10}$  bacteria  $\text{mL}^{-1}$  produced a maximum angular speed of 4 rpm,<sup>22</sup> and swarming dense *Vibrio alginolyticus* bacteria produced a maximum angular speed of 7 rpm.<sup>24</sup> Carefully-designed 3-D microrotors, designed to capture up to 15 swimming cells within microchambers at the rotor edge, rotated at speeds of up to 20 rpm.<sup>23</sup> Rotors in these examples, however, were required to be chiral to exploit the breaking of detailed balance in active baths<sup>25</sup> and generate directional motion.

By contrast, the use of active fluids to move non-rigid liquid droplets, for which surface tension imposes a spherically

symmetric shape, remains understudied. It is well established that emulsions can be made to move through addition of surfactants, which generate interfacial Marangoni stresses that drive self-sustaining motion.<sup>26–36</sup> Symmetry is broken through the spatial gradient of surfactants on the droplet surface.<sup>26,31</sup> Rotational torque can be generated by coupling the surfactant-induced surface flows to nematic order in a confined liquid crystal.<sup>37</sup> Fewer studies, however, have investigated droplet motion driven by active fluids. Molecular motors confined with microtubules inside droplets can generate internal vortex formation.<sup>38</sup> Likewise, bacteria confined within droplets can generate internal vortices.<sup>39</sup> These studies do not directly investigate motion of the drop itself. Bundles of active microtubules that adsorb to the internal oil–water interface can drive droplet translation.<sup>4</sup> Nonetheless, examples of droplet motion driven by external active fluids, including bacteria, remain infrequent.

Here, we show that active, adherent flagellated bacteria can drive rotation of spherical liquid droplets near a liquid–solid interface. We characterize adhesion of bacteria using confocal microscopy and analyze droplet motion using brightfield microscopy and particle tracking. Symmetry-breaking hydrodynamic interactions of bacteria with the nearby liquid–solid interface lead to clockwise rotation of the droplets when viewed from the liquid side. The rotation rate scales approximately inversely with the droplet radius, consistent with a physical picture in which bacteria randomly attached at the droplet surface drive the rotation. The speed of rotation can be tuned by changing the number of adherent bacteria, through variations in cell concentration, bacterial species, or surfactant concentration. By showing how active bacteria can be used to drive the directional rotation of non-chiral, spherically symmetric droplets, this study opens a route to manipulate fluid droplets in an active bath.

Department of Chemical and Biomolecular Engineering, University of Houston, Houston, TX 77204, USA. E-mail: jconrad@uh.edu

† Electronic supplementary information (ESI) available. See DOI: 10.1039/c9sm01570a

## 2 Materials and methods

### 2.1 Chemicals

Dodecane ( $\geq 99\%$ , Sigma-Aldrich), hexadecane ( $\geq 99\%$ , Sigma-Aldrich), 1  $\mu\text{m}$  FluoSpheres sulfate microspheres (Thermo-Fisher), potassium nitrate ( $\geq 99\%$ , EMD), Zobell marine broth 2216 (HiMedia Lab), sodium pyruvate (Amresco), SYTO9 (Thermo-Fisher), ethylene glycol (Sigma-Aldrich), and diiodomethane (Sigma-Aldrich) were used as received.

### 2.2 Bacteria strains

We used two motile bacteria isolated from the Gulf of Mexico during the Deepwater Horizon oil spill, obtained from Dr Romy Chakraborty and Dr Gary Anderson (Lawrence Berkeley National Laboratory) via Dr Douglas Bartlett (Scripps Institute of Oceanography, UCSD). Bead 10BA (isolated from 1509 m) is related to *Halomonas titanicae*. *H. titanicae* is a moderately halophilic, Gram-negative marine bacterium. These bacteria are rod-shaped, roughly 0.5–0.8  $\mu\text{m}$  in diameter and 1.5–6  $\mu\text{m}$  in length, and swim using their peritrichous flagella.<sup>40</sup>

Bead B37B (isolated from 150 m) is related to *Shewanella haliotis* strain DW01. *S. haliotis* is Gram-negative, rod-shaped, and 0.5–0.7  $\mu\text{m}$  in diameter and 2.0–4.3  $\mu\text{m}$  in length.<sup>41</sup> *Shewanella* species typically swim using a single polar flagellum.<sup>42,43</sup> The two Gulf bacteria are hereafter referred to by their closest species name.

In addition to the Gulf isolates, we also examined one model motile bacterium. *Escherichia coli* MC1061, provided by Dr Patrick Cirino (University of Houston), is Gram-negative, rod-shaped, and 0.7–0.9  $\mu\text{m}$  in diameter and 2.0–3.0  $\mu\text{m}$  in length and swims by bundling its peritrichous flagella.

### 2.3 Growth conditions

*H. titanicae* and *S. haliotis* were streaked from a frozen stock on a marine agar plate (37.4 g L<sup>-1</sup> marine broth, 10 g L<sup>-1</sup> sodium pyruvate, 15 g L<sup>-1</sup> agar) and incubated at 30 °C for 40 h. A single colony selected from these plates was inoculated into 20 mL of culture medium (37.4 g L<sup>-1</sup> marine broth and 10 g L<sup>-1</sup> pyruvate) and incubated for 20 h in an orbital incubator shaker (New Brunswick Scientific) at 200 rpm and 30 °C. Finally, a subculture was prepared by inoculating 60  $\mu\text{L}$  of the principal culture into 20 mL of culture medium and grown to late exponential phase in an orbital incubator shaker at 30 °C and 200 rpm for 20 h. *E. coli* was streaked on a Luria-Bertani agar plate and cultured in Luria-Bertani medium at 37 °C and 250 rpm for 12 h.

### 2.4 Preparation of glass capillaries for imaging

Thin rectangular borosilicate capillaries (0.1 mm height, 1 mm width, 50 mm length, 0.07 mm wall thickness, Vitrocom) were used as sample chambers in imaging experiments. To minimize adhesion of bacteria and prevent wetting of oil drops, the capillaries were made hydrophilic by plasma treatment (Harrick plasma cleaner PDC-32G) using oxygen plasma for 2 minutes. The plasma-treated surface was fully wetted by water when the water contact angle was measured using a DataPhysics OCA 15EC contact angle goniometer. This hydrophilic surface prevented

adhesion of cells and droplets on the inner surface of the glass capillary. The plasma-treated capillaries were immediately filled with the droplet-cell suspension for imaging to minimize any change in surface hydrophilicity during the experiment.

### 2.5 Zeta potential and surface energy

Cells were grown to late exponential phase for surface characterization. 20 mL of each bacteria suspension was centrifuged at 5000g for 10 minutes in a Sorvall ST 16 Centrifuge (Thermo Fisher Scientific). The resultant pellet was resuspended in 20 mL MilliQ water and centrifuged again. The process was repeated one more time and the final pellet was resuspended in MilliQ water. The final optical density at 600 nm (OD<sub>600nm</sub>) was adjusted to 0.04 (Laxco DSM-Micro Cell Density Meter) with MilliQ water.<sup>44</sup>

The zeta potentials of the bacteria suspensions and particle suspension were measured using a Nicomp 380  $\zeta$ -potential analyzer (Table S1 in the ESI<sup>†</sup>). For measurements of the surface energy, the bacteria suspension (OD 1.0 in MilliQ water) was filtered through cellulose acetate membrane filters (pore diameter 0.45  $\mu\text{m}$ , Advantec) under vacuum at 100 mm Hg below atmospheric pressure using a GEM 8890 vacuum pump (Welch).<sup>45</sup> The contact angles for three liquids (MilliQ water, ethylene glycol and diiodomethane) were measured on the lawns using a Dataphysics OCA 15EC goniometer. The surface energy of the bacteria was calculated from inbuilt software using the method of Wu.<sup>46,47</sup> Contact angle and surface energy data are provided in Table S2 in the ESI<sup>†</sup>.

### 2.6 Brightfield imaging assay for drop rotation

For imaging experiments, cells were harvested at late exponential phase. 10 mL of the cell suspension was centrifuged at 2000g for 10 min to remove the medium and the pellet was resuspended in 10 g L<sup>-1</sup> of potassium nitrate solution prepared in MilliQ water. Separately, emulsions of dodecane in potassium nitrate solution were made by shaking 20  $\mu\text{L}$  of dodecane (or hexadecane; the IFT values are provided in Table S3 in the ESI<sup>†</sup>) in 300–400  $\mu\text{L}$  of KNO<sub>3</sub> solution. To these emulsions, 25  $\mu\text{L}$  of PS particles (0.04% v/v) were added and the suspension shaken again. Using this technique, we obtained drops of diameter 10–100  $\mu\text{m}$  (Fig. S1 in the ESI<sup>†</sup>). The PS particles were added to aid in the determination of the angular position of the drop over time. We selected the particle concentration such that only 1–4 particles attached to the dodecane/water interface. We confirmed that the PS particles attached to the droplet/water interface using confocal microscopy (Fig. S2 in the ESI<sup>†</sup>).

The final suspension was prepared by adding 100–200  $\mu\text{L}$  of cell suspension to an Eppendorf tube. Through this protocol, we generated bacterial suspensions with optical densities of 0.3–3, corresponding to number concentrations of  $8.1 \times 10^8$  cells mL<sup>-1</sup> to  $8.1 \times 10^9$  cells mL<sup>-1</sup> for *H. titanicae*; optical density of 1.0, corresponding to number concentration of  $2.7 \times 10^9$  cells mL<sup>-1</sup>, for *E. coli*; and optical density of 0.31, corresponding to number concentration of  $2.7 \times 10^9$  cells mL<sup>-1</sup>, *S. haliotis*. The OD was adjusted to obtain the same number density for comparisons between different species. These concentrations are lower

than those typically required to obtain collective swimming ( $\sim 10^{10}$  cells  $\text{mL}^{-1}$  (ref. 21)).

Finally, 6.7  $\mu\text{L}$  of the emulsion-bacteria suspension was injected into a glass microfluidic channel and both ends of the channel were sealed with vacuum grease. The droplets, whose density was lower than that of water, were preferentially located at the top wall of the capillary, within one micron of the surface. Occasionally, a droplet remained near the bottom surface due to an interaction with the substrate.

We used a brightfield inverted microscope (Leica Microsystems DM4000) equipped with a 40 $\times$  objective lens (HCX PL APO, NA 1.25–0.75) to image rotating droplets. Images of droplets located at least 400  $\mu\text{m}$  away from the side walls of the capillaries, to avoid any interference from the lateral walls, were acquired for up to ten minutes after injection to ensure that the capillary surface remained hydrophilic throughout the measurement; we note that droplet rotation persisted for more than two hours (Fig. S3 in the ESI $^\dagger$ ). Images were captured at a rate of 5 frames  $\text{s}^{-1}$  for 60 s using a digital camera (Olympus DP21). To analyze the drop rotation, we tracked the positions of the PS particles attached to the droplet interface using algorithms written in Matlab. We determined the angular speed of individual droplets from the slope of total rotation as a function of time over at least 20 s.

### 2.7 Confocal imaging assay for cell adhesion

Bacterial suspensions for confocal imaging were prepared similarly to those for the rotation assay, except that PS particles were not added and cells were stained with SYTO9 (Thermo-Fisher) following our standard protocol.<sup>48</sup> Cells were imaged in 3-D by acquiring sequential 2-D images separated by a vertical step  $\Delta z = 0.31$   $\mu\text{m}$  using a VT-Infinity (Visitech, Sunderland, UK) confocal microscope equipped with the aforementioned 40 $\times$  lens. Each image stack, containing 193 images, was merged into a single 2-D image to obtain a visual representation of cell density on droplet surface. We acquired five z-stacks of droplets for three independent cultures for each OD. We enumerated the number of cells adhered on each droplet manually using ImageJ software.

## 3 Results and discussion

### 3.1 Droplet rotation by *H. titanicae*

Dodecane droplets in a concentrated suspension of *H. titanicae* bacteria rotate clockwise over time, as shown for a droplet of diameter 40  $\mu\text{m}$  located near the top surface of the capillary in Fig. 1(a). The optical density  $\text{OD}_{600\text{nm}}$  of the suspension was 1.0, corresponding to a number density of  $2.7 \times 10^9$  cells  $\text{mL}^{-1}$ . The droplet rotates steadily over 10 s (Movies S1–S3 in ESI $^\dagger$ ). Bacteria appear to strongly adhere to the surface of the oil droplets and do not swim when attached, as indicated by their lack of relative rearrangement on the interface over time (Movie S1, ESI $^\dagger$ ). Conversely, a droplet of similar diameter does not rotate when placed in a bacterial suspension of lower concentration (optical density  $\text{OD}_{600\text{nm}} = 0.03$ ) (Fig. 1(b)). We varied the concentration of bacteria across three orders of magnitude in

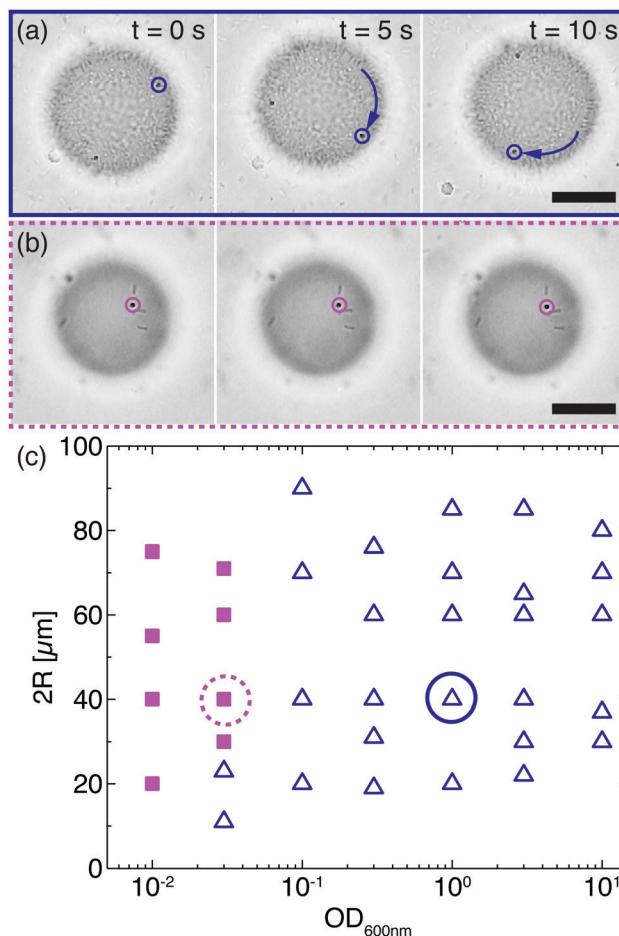
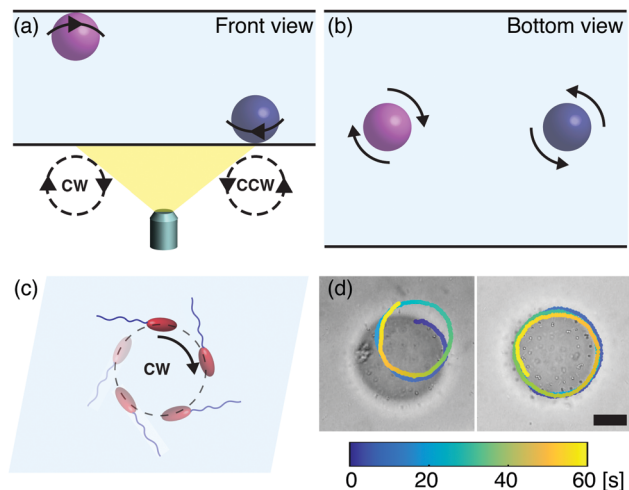


Fig. 1 (a and b) Micrographs of droplets at 0, 5 and 10 s in suspensions of *H. titanicae* at  $\text{OD}_{600\text{nm}}$  of (a) 1.0 and (b) 0.03. Arrows indicate the net rotation between images. The scale bar is 20  $\mu\text{m}$ . (c) State diagram for rotation of dodecane droplets in *H. titanicae* suspensions containing 10  $\text{g L}^{-1}$  potassium nitrate as a function of drop diameter  $2R$  and bacterial optical density ( $\text{OD}_{600\text{nm}}$ ). A state point was considered to be non-rotating if all droplets moved less than  $2^\circ$  in 30 s ( $n \geq 10$  droplets for each state point). Squares and triangles respectively indicate non-rotating and rotating droplets.

optical density, which also altered the cell concentration on the droplet surface (Fig. S4 in ESI $^\dagger$ ), and the droplet diameter by a factor of five. Generally, droplets do not rotate when the concentration of bacteria is below  $\text{OD}_{600\text{nm}} \approx 10^{-1}$  except for the smallest droplets examined (Fig. 1(c)). We therefore conclude that rotation is driven by activity of the bacteria.

These experiments are carried out in a microchannel of height 100  $\mu\text{m}$ . Although most (low-density) oil droplets are located near the top of the microchannel, a few droplets remain near the bottom channel surface. Droplets near each surface rotate in a consistent direction: clockwise near the top surface and counter-clockwise near the bottom surface, as shown for representative droplets and schematically in Fig. 2. This rotation is due to hydrodynamic interaction of the bacteria flagella with the solid wall. A bacterium located above a wall swims in a clockwise direction, due to these hydrodynamic interactions.<sup>49,50</sup> Bacteria adhering to a droplet experience similar hydrodynamic



**Fig. 2** (a and b) Schematic illustrating the direction of rotation of droplets located near the top and bottom surfaces as viewed from the (a) front and (b) bottom. (c) Schematic illustrating the clockwise trajectory of a bacterium located near a solid surface, viewed from above (liquid side). (d) Clockwise (left) and counter-clockwise (right) rotation of droplets as revealed from the trajectories of PS particles, overlaid onto micrographs of the droplets of at the start of the movie. The scale bar is 20  $\mu\text{m}$ .

interactions. Because the cells are adhered to the interface, the torque generated by their flagella is transferred to the droplets, driving the droplet to rotate in a consistent direction. This mechanism is similar to that proposed for the directional bias in rotation of a planar square driven by adherent bacteria<sup>16</sup> and of clusters of bacteria.<sup>51</sup>

### 3.2 Angular speed of rotation

To characterize the effect of bacterial activity on droplet rotation, we add PS microparticles to suspensions of *H. titanicae* bacteria and dodecane droplets (20–95  $\mu\text{m}$  diameter) in aqueous solutions of  $\text{KNO}_3$ . The PS particles strongly adhere to the dodecane-water interface but do not attach to the negatively-charged cells, so that their motion can be tracked over time (Fig. 3). We also track the motion of the droplet centroid, which was calculated from the average position of the oil-water interface at a given time. From the trajectory of the droplet centroid, we calculate the droplet mean-square displacement (MSD) as a function of time (Fig. S5 in the ESI†). The MSD for droplets of similar size varies markedly (Fig. S6 in the ESI†). This variation likely results from differences in the interactions of droplets with the nearby wall, and is not discussed further.

The angular displacement of droplets increases linearly with time (Fig. 3(b)). We extract the angular speed  $\omega$  from a linear fit of the angular displacement as a function of time. The maximum speed of rotation observed here, 7.5 rpm for 20  $\mu\text{m}$  diameter droplets, is comparable to speeds measured for microscale objects rotated by free-swimming, trapped, or adherent bacteria. For example, collectively-swimming bacteria drove rotation of a hexagonal microrotor of side length 10  $\mu\text{m}$  at 2 rpm,<sup>20</sup> and of microgears of diameter 24 and 48  $\mu\text{m}$  at 7.1 rpm<sup>24</sup> and 4 rpm,<sup>22</sup> respectively. Swimming bacteria trapped within microcavities on a micromotor of diameter 15.2  $\mu\text{m}$  rotated at 20 rpm.<sup>23</sup> Finally,

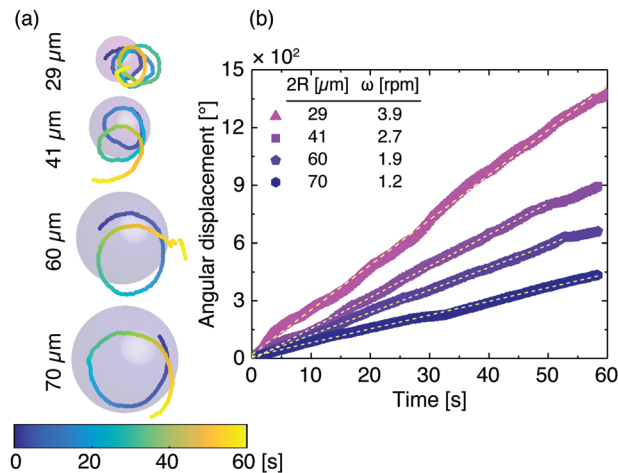


**Fig. 3** (a) Representative trajectories of PS particles adhered on the surface of dodecane droplets of diameter 29, 41, 60, or 70  $\mu\text{m}$  suspended in 10  $\text{g L}^{-1}$  potassium nitrate in water. Color indicates time; the underlaid circles indicate the initial position and diameter 2R of droplets. (b) Net rotation of droplets shown in (a) as a function of time. The corresponding speed of rotation, in rotations per minute (rpm), is provided in the inset. The  $\text{OD}_{600\text{nm}}$  of the cell suspension prior to mixing of the oil droplets was 1.0.

bacteria adhered to a square of side length 60  $\mu\text{m}$  drove rotation at 1.3 rpm.<sup>16</sup>

The angular speed  $\omega$  decreases as the droplet size is increased (Fig. 4). A similar decrease in  $\omega$  with increasing  $R$  is also observed for bacteria on hexadecane droplets (Fig. S7 in the ESI†). The change in angular speed reflects two factors: the number of adherent bacteria, which in our earlier work depended on drop size,<sup>48</sup> and the drag force on a rotating droplet, which increases with the drop diameter.<sup>52,53</sup> We systematically explore these effects, starting with the concentration of bacteria in suspension. The angular speed  $\omega$  of droplets of similar diameter

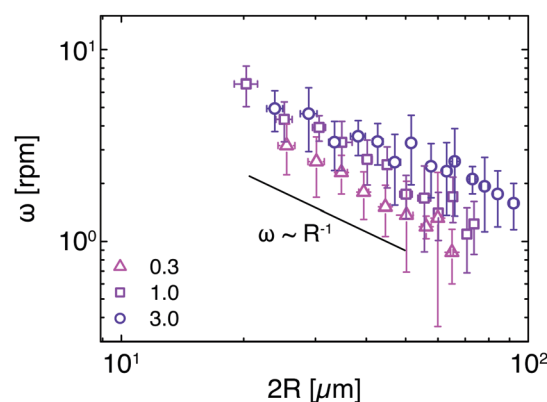


**Fig. 4** Angular speed of dodecane droplets in 10  $\text{g L}^{-1}$  potassium nitrate in MilliQ water as a function of droplet diameter 2R. Symbols indicate different concentrations of bacteria, with OD 0.3 (triangles), 1.0 (squares), or 3.0 (circles). Data points indicate the average and standard deviation over  $n = 3$  to 18 droplets whose diameters fell within 4  $\mu\text{m}$  (scatter plot Fig. S8 in the ESI†). The solid line indicates a power-law with exponent  $-1$ . The  $R^2$  values of the fits are 0.95, 0.93, and 0.84 for ODs of 0.30, 1.0, and 3.0, respectively.

increases less than linearly with the optical density (Fig. 4). As the optical density is varied by one order of magnitude,  $\omega$  varies by a factor of 2 to 3 depending on the droplet diameter. Because the standard deviation of  $\omega$  is large, this variation may fall within statistical errors for certain droplet diameters (e.g., 30  $\mu\text{m}$ ).

The optical density is a measure of the concentration of bacteria in suspension, but does not necessarily proportionally scale with the number of bacteria at the oil–water interface.<sup>48</sup> To relate the number of bacteria at the interface to the optical density, we count the number of bacteria directly adhered to the interface in 3-D confocal micrographs (Fig. 5). The number of cells on the droplet surface increases by  $30 \pm 3\%$  ( $n = 15$ ) as the  $\text{OD}_{600\text{nm}}$  is increased from 0.3 to 3.0. Assuming that attached bacteria are randomly oriented on the surface, the net propulsive force exerted by  $N$  bacteria is expected to scale as  $N^{1/2}$ .<sup>11–13,51</sup> We find, however, that the percentage increase in  $N^{1/2}$  ( $14 \pm 1\%$ ,  $n = 15$ ) is lower than the percentage increase in angular speed ( $77 \pm 47\%$ ,  $n > 10$ ). (The large errors on the angular speed likely reflect differences in the interactions between droplets and the nearby capillary surface, which also affect the MSD.) This result suggests that cells in suspension begin to contribute to droplet rotation as the concentration is increased.

As a first step towards understanding how bacteria drive droplet rotation, we consider droplet rotation propelled by cells attached to the droplet surface. The torque counteracting frictional rotational drag<sup>52,53</sup> on a droplet is given by  $T_{\text{drag}} = 8\pi\mu R^3\omega$ , where  $R$  is the radius of the droplet and  $\mu$  is the solution viscosity. This rotational drag is balanced by the net torque exerted by attached bacteria. For  $N$  randomly-oriented bacteria, the net torque scales as  $T_{\text{net}} = F_a N^{1/2} R$ , where  $F_a$  is the propulsive force from one bacterium. In our earlier experiments the number of adherent cells scaled approximately with the droplet surface area, such that  $N^{1/2} \propto R$ .<sup>48</sup> Equating these two expressions suggests that  $\omega \propto R^{-1}$ . Our data at the two lowest OD values (0.30 and 1.0) are consistent with this scaling (Fig. 4), as indicated by  $R^2$  values of 0.95 and 0.93 for a fit to  $\omega \sim R^{-1}$ . At higher OD = 3.0, however,  $\omega$  decreases less rapidly than  $R^{-1}$ , as confirmed by the  $R^2$  value of 0.84, indicating that droplets rotate slightly faster than expected from their size. This result suggests that collective swimming effects may become important at number densities approaching  $10^{10}$  cells  $\text{mL}^{-1}$  for *H. titanicae*.

The scaling expression  $\omega \propto R^{-1}$  approximates a bacterium as a force monopole. Because swimming bacteria must exert

zero total force on the fluid, a bacterium should be approximated to lowest order as a force dipole.<sup>54,55</sup> A correction to the net torque, derived in ref. 51, was obtained by considering the propulsive force exerted by a flagellum, which generates an additional drag force that acts on a rotating object. The torque exerted by a bacterium, accounting for this dipole correction, is given by  $T_{\text{net}} \propto N^{1/2} R [1 - R(l^2 + R^2)^{-1/2}]$ , where  $l$  is the length of a flagellum.<sup>51</sup> The dipole torque model, however, less accurately captures the droplet size dependence of  $\omega$  than does the monopole torque model (Fig. S9 in ESI†), likely because the droplet size remains comparable to the flagellum length  $l \approx 10 \mu\text{m}$ . The viscous drag due to a nearby wall leads to a numerical correction but to lowest order does not alter the  $R$ -scaling of the net torque at low Reynolds number;<sup>56</sup> this correction is of order 15% for a droplet of radius 15  $\mu\text{m}$  that is located 1  $\mu\text{m}$  from the wall.<sup>57</sup>

### 3.3 Tuning rotation through interfacial tension

The results presented in Fig. 1–5 reveal that the rotation of droplets is driven by adherent bacteria. This result suggests that modifying the interaction between bacteria and the interface will alter the rotation behavior. To test this idea, we examine the effect of the oil–water interfacial tension on drop rotation. We use an anionic surfactant, dioctyl sodium sulfosuccinate (DOSS), to modify the interfacial tension between dodecane and water. We previously showed that increasing the surfactant concentration decreased the interfacial tension of dodecane–water (Fig. S10 in the ESI†), which increased the free energy of adhesion and thereby reduced adhesion of cells to droplets.<sup>48</sup> Thus, changing the concentration of DOSS is expected to alter bacteria-driven rotation of droplets.

We observe droplet rotation driven by *H. titanicae* for DOSS concentrations in the range 0–3500 ppm (Fig. 6 and Movie S4 for [DOSS] = 3500 ppm, ESI†). The angular speed of droplets appears to decrease with increasing surfactant concentration above 100 ppm. Because the interfacial tension decreases as the concentration of DOSS is increased, the PS particles do not strongly adhere to the droplet interface, as indicated by changes in their relative positions on the interface over time. The bacteria also appear to rearrange relative to others over time, suggesting that they are able to swim while attached to the DOSS-decorated interfaces. Thus, the movement of the PS particles does not quantitatively capture the droplet angular speed. Indeed, at high DOSS concentration the PS particles move much faster than the droplet, so that the droplet angular speed cannot be accurately measured. Two mechanisms may

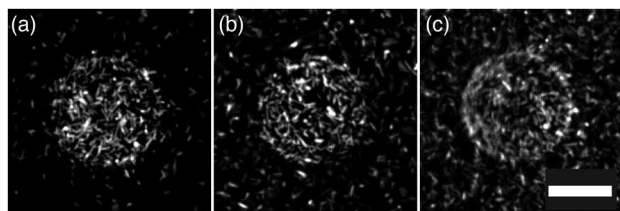


Fig. 5 2-D projection of 3-D images of *H. titanicae* cells on 30  $\mu\text{m}$  dodecane drop interfaces at optical densities of (a) 0.3, (b) 1.0, and (c) 3.0 captured using confocal microscopy. The number of attached cells is  $284 \pm 16$ ,  $363 \pm 20$ , and  $368 \pm 23$  for OD of 0.3 ( $n = 15$  droplets), 1.0 ( $n = 15$  droplets), and 3.0 ( $n = 15$  droplets), respectively. The scale bar is 20  $\mu\text{m}$ .

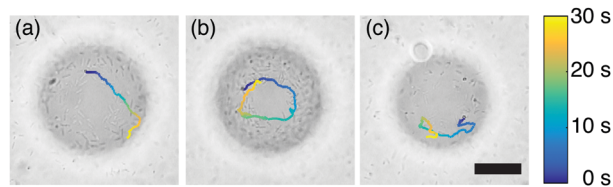


Fig. 6 PS particle trajectories on rotating droplets as a function of DOSS concentration: (a) 50 ppm, (b) 200 ppm, and (c) 500 ppm. The scale bar is 20  $\mu\text{m}$ .

contribute to the apparent decrease in droplet angular speed as the surfactant concentration is increased. First, fewer cells adhere to the interface due to the lower interfacial tension,<sup>48</sup> thereby reducing the total torque. A similar mechanism was shown in ref. 16, in which adding surfactants removed the cells attached to a microgear that drove its motion. Second, adding surfactant also reduces the strength of adhesion of cells at the droplet interface. In support of this idea, cells swim more at the interface as the surfactant concentration is increased. We propose that less-strongly adhered cells transmit force less efficiently to the droplet, again reducing the net torque.

### 3.4 Tuning rotation through interfacial affinity

Finally, we characterize droplet rotation for three species of motile bacteria, monotrichous *S. haliotis* and peritrichous *E. coli* and *H. titanicae*. All three bacteria readily swim in the aqueous salt solution, with average near-surface speeds of  $13 \pm 2$ ,  $10 \pm 3$ , and  $10 \pm 4 \mu\text{m s}^{-1}$  for *E. coli*, *S. haliotis*, and *H. titanicae*, respectively. The swimming speed is approximately constant despite different numbers of flagella in the three species, consistent with experimental observations<sup>58</sup> and a theoretical model.<sup>59</sup> The surface energies of the three strains are 66, 66, and

$64 \text{ mN m}^{-1}$  for *E. coli*, *S. haliotis*, and *H. titanicae*, respectively. The angular speed of  $40 \mu\text{m}$  droplets, determined from the trajectories of PS particles adhered to the oil–water interface (Fig. 7(a–c)), increases from 0.1 rpm for *E. coli* to 2.5 rpm for *H. titanicae* (Fig. 7(a)).

Confocal micrographs reveal that very few *E. coli* adhere to the oil–water interface (Fig. 7(e)). Thus, the slow rotation for this species is likely due to the low number of bacteria propelling the droplet. Although *S. haliotis* bacteria adhere at the interface in slightly lower numbers as compared to *H. titanicae* (Fig. 7(f and g)), droplets propelled by *S. haliotis* rotate twelve times slower than those driven by *H. titanicae*. Increasing the concentration of *S. haliotis* increases the droplet rotation speed (Fig. S11 in the ESI†). Movies of *S. haliotis* indicate that these bacteria are more motile at the interface than *H. titanicae*. We therefore speculate that the relatively slow rotation of *S. haliotis*-driven droplets results from the weaker interfacial adhesion.

## 4 Conclusions

We examined the effect of droplet diameter, cell concentration, oil–water interfacial tension, and bacteria species on the directional rotation of droplets near a liquid–solid interface. Droplets begin to rotate when the concentration of bacteria is increased above a certain optical density. Variation in droplet rotational speed reflects differences in the number of bacteria adhered at the droplet interface. The angular speed of droplets decreases with increasing droplet diameter, consistent with a physical picture in which rotation of flagella of randomly-oriented bacteria generates a torque on the droplets. The speed of rotation can be tuned through the number of bacteria adhered to the interface, by varying surfactant concentration or bacterial species.

The clockwise rotation, as viewed from the liquid side, is driven by the hydrodynamic interactions of flagella with the nearby surface. This mechanism, arising from interactions of bacteria confined near a surface,<sup>60</sup> enables directional rotation of a symmetric object to be generated from active suspensions, in contrast to symmetry-breaking through object chirality<sup>20–23</sup> or non-uniform bacterial adhesion.<sup>13,61</sup> Bacteria-driven droplet rotation may provide a route to enhance mixing and thereby promote mass transport in multiphase microbial reactors<sup>62</sup> or drive cells to agglomerate at the droplet surface through hydrodynamic interactions.<sup>63,64</sup> Thus the ability to actively drive droplet rotation may be useful in a variety of practical settings involving microbes.

In addition, active particles can exhibit a wide range of interesting collective behaviors. For example, self-propelled droplets can form clusters that collectively translate and rotate when confined.<sup>65,66</sup> Whether droplets driven by adhered bacteria exhibit collective motion at high densities is an open question for future study.

## Conflicts of interest

There are no conflicts to declare.

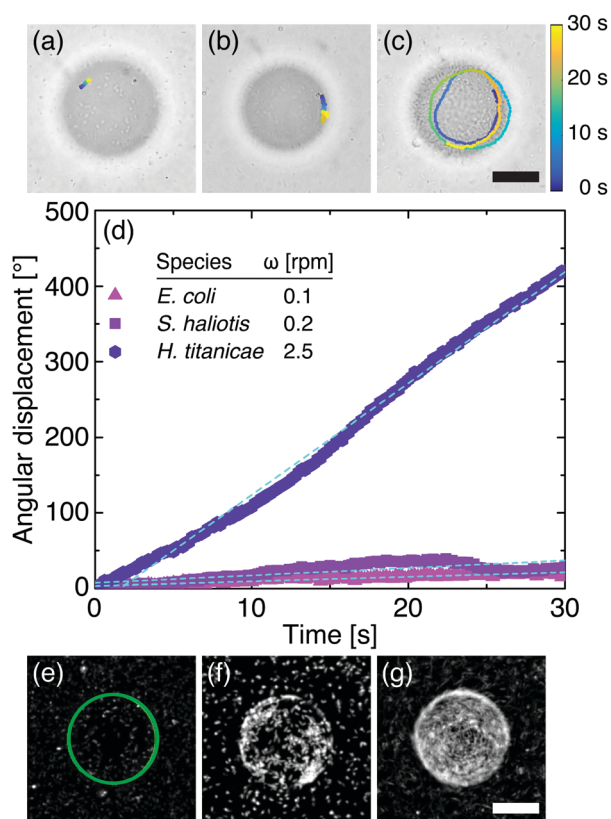


Fig. 7 Trajectories of a PS particle on the interface of a dodecane droplets of diameter  $40 \mu\text{m}$  in the presence of (a) *E. coli*, (b) *S. haliotis*, and (c) *H. titanicae* bacteria at cell concentration  $=2.7 \times 10^9 \text{ cells mL}^{-1}$ . (d) Angular displacement as a function of time for the three species. The inset table provides the rotation rate, determined from the slope. (e–g) 2-D projections of 3-D images, obtained using confocal microscopy, for (e) *E. coli*, (f) *S. haliotis*, and (g) *H. titanicae*. The scale bars in (c) and (g) are  $20 \mu\text{m}$ .

## Acknowledgements

This research was made possible in part by a grant from The Gulf of Mexico Research Initiative, and in part by the Welch Foundation (E-1869). Data generated for this paper is available on the Gulf of Mexico Research Initiative Information and Data Cooperative (GRIIDC) at <https://data.gulfresearchinitiative.org> (DOI: 10.7266/n7-k407-eb54). We thank Dr Douglas Bartlett (UCSD) for providing marine bacteria strains and Dr Patrick Cirino (UH) for providing the *E. coli* strain.

## References

- 1 S. Ramaswamy, *Annu. Rev. Condens. Matter Phys.*, 2010, **1**, 323–345.
- 2 G. H. Koenderink, Z. Dogic, F. Nakamura, P. M. Bendix, F. C. MacKintosh, J. H. Hartwig, T. P. Stossel and D. A. Weitz, *Proc. Natl. Acad. Sci. U. S. A.*, 2009, **106**, 15192–15197.
- 3 T. Thoresen, M. Lenz and M. L. Gardel, *Biophys. J.*, 2011, **100**, 2698–2705.
- 4 T. Sanchez, D. T. N. Chen, S. J. DeCamp, M. Heymann and Z. Dogic, *Nature*, 2012, **491**, 431–434.
- 5 F. C. Keber, E. Loiseau, T. Sanchez, S. J. DeCamp, L. Giomi, M. J. Bowick, M. C. Marchetti, Z. Dogic and A. R. Bausch, *Science*, 2014, **345**, 1135–1139.
- 6 M. D. Manson, P. Tedesco, H. C. Berg, F. M. Harold and C. Van der Drift, *Proc. Natl. Acad. Sci. U. S. A.*, 1977, **74**, 3060–3064.
- 7 D. Owen, M. Ballard, A. Alexeev and P. J. Hesketh, *Sens. Actuators, A*, 2016, **251**, 84–91.
- 8 D. Akin, J. Sturgis, K. Ragheb, D. Sherman, K. Burkholder, J. P. Robinson, A. K. Bhunia, S. Mohammed and R. Bashir, *Nat. Nanotechnol.*, 2007, **2**, 441–449.
- 9 O. Felfoul, M. Mohammadi, S. Taherkhani, D. De Lanauze, Y. Z. Xu, D. Loghin, S. Essa, S. Jancik, D. Houle and M. Lafleur, *et al.*, *Nat. Nanotechnol.*, 2016, **11**, 941–947.
- 10 B.-W. Park, J. Zhuang, O. Yasa and M. Sitti, *ACS Nano*, 2017, **11**, 8910–8923.
- 11 N. Darnton, L. Turner, K. Breuer and H. C. Berg, *Biophys. J.*, 2004, **86**, 1863–1870.
- 12 B. Behkam and M. Sitti, *Appl. Phys. Lett.*, 2007, **90**, 023902.
- 13 B. Behkam and M. Sitti, *Appl. Phys. Lett.*, 2008, **93**, 223901.
- 14 E. B. Steager, M. S. Sakar, D. H. Kim, V. Kumar, G. J. Pappas and M. J. Kim, *J. Micromech. Microeng.*, 2011, **21**, 035001.
- 15 A. Sahari, D. Headen and B. Behkam, *Biomed. Microdevices*, 2012, **14**, 999–1007.
- 16 D. Wong, E. E. Beattie, E. B. Steager and V. Kumar, *Appl. Phys. Lett.*, 2013, **103**, 153707.
- 17 A. Sahari, M. A. Traore, B. E. Scharf and B. Behkam, *Biomed. Microdevices*, 2014, **16**, 717–725.
- 18 M. M. Stanton and S. Sánchez, *Trends Biotechnol.*, 2017, **35**, 910–913.
- 19 L. Vaccari, M. Molaei, R. L. Leheny and K. J. Stebe, *Soft Matter*, 2018, **14**, 5643–5653.
- 20 Y. Hiratsuka, M. Miyata, T. Tada and T. Q. Uyeda, *Proc. Natl. Acad. Sci. U. S. A.*, 2006, **103**, 13618–13623.
- 21 A. Sokolov, M. M. Apodaca, B. A. Grzybowski and I. S. Aranson, *Proc. Natl. Acad. Sci. U. S. A.*, 2010, **107**, 969–974.
- 22 R. Di Leonardo, L. Angelani, D. Dell'Arciprete, G. Ruocco, V. Iebba, S. Schippa, M. P. Conte, F. Mecarini, F. De Angelis and E. Di Fabrizio, *Proc. Natl. Acad. Sci. U. S. A.*, 2010, **107**, 9541–9545.
- 23 G. Vizsnyiczai, G. Frangipane, C. Maggi, F. Saglimbeni, S. Bianchi and R. Di Leonardo, *Nat. Commun.*, 2017, **8**, 15974.
- 24 M. Kojima, T. Miyamoto, M. Nakajima, M. Homma, T. Arai and T. Fukuda, *Sens. Actuators, B*, 2015, **222**, 1220–1225.
- 25 M. E. Cates, *Rep. Prog. Phys.*, 2012, **75**, 042601.
- 26 F. Brochard, *Langmuir*, 1989, **5**, 432–438.
- 27 T. Toyota, H. Tsuha, K. Yamada, K. Takakura, T. Ikegami and T. Sugawara, *Chem. Lett.*, 2006, **35**, 708–709.
- 28 S. Thutupalli, R. Seemann and S. Herminghaus, *New J. Phys.*, 2011, **13**, 073021.
- 29 T. Banno, R. Kuroha and T. Toyota, *Langmuir*, 2012, **28**, 1190–1195.
- 30 K. Peddireddy, P. Kumar, S. Thutupalli, S. Herminghaus and C. Bahr, *Langmuir*, 2012, **28**, 12426–12431.
- 31 S. Herminghaus, C. C. Maass, C. Krüger, S. Thutupalli, L. Goehring and C. Bahr, *Soft Matter*, 2014, **10**, 7008–7022.
- 32 S. Tanaka, Y. Sogabe and S. Nakata, *Phys. Rev. E: Stat., Nonlinear, Soft Matter Phys.*, 2015, **91**, 032406.
- 33 C. Jin, C. Krüger and C. C. Maass, *Proc. Natl. Acad. Sci. U. S. A.*, 2017, **114**, 5089–5094.
- 34 Y. Nagasaka, S. Tanaka, T. Nehira and T. Amimoto, *Soft Matter*, 2017, **13**, 6450–6457.
- 35 J. Čejková, T. Banno, M. M. Hanczyc and F. Štěpánek, *Artif. Life*, 2017, **23**, 528–549.
- 36 M. Suga, S. Suda, M. Ichikawa and Y. Kimura, *Phys. Rev. E*, 2018, **97**, 062703.
- 37 C. Krüger, G. Klös, C. Bahr and C. C. Maass, *Phys. Rev. Lett.*, 2016, **117**, 048003.
- 38 K. Suzuki, M. Miyazaki, J. Takagi, T. Itabashi and S. Ishiwata, *Proc. Natl. Acad. Sci. U. S. A.*, 2017, **114**, 2922–2927.
- 39 E. Lushi, H. Wioland and R. E. Goldstein, *Proc. Natl. Acad. Sci. U. S. A.*, 2014, **111**, 9733–9738.
- 40 J.-C. Lee, Y.-S. Kim, B.-S. Yun and K.-S. Whang, *Int. J. Syst. Evol. Microbiol.*, 2015, **65**, 4792–4799.
- 41 D. Kim, K. S. Baik, M. S. Kim, B.-M. Jung, T.-S. Shin, G.-H. Chung, M. S. Rhee and C. N. Seong, *Int. J. Syst. Evol. Microbiol.*, 2007, **57**, 2926–2931.
- 42 P. Verma, P. K. Pandey, A. K. Gupta, H. J. Kim, K. S. Baik, C. N. Seong, M. S. Patole and Y. S. Shouche, *Int. J. Syst. Evol. Microbiol.*, 2011, **61**, 2058–2064.
- 43 S.-J. Kim, S.-J. Park, Y.-S. Oh, S.-A. Lee, K.-S. Shin, D.-H. Roh and S.-K. Rhee, *Int. J. Syst. Evol. Microbiol.*, 2012, **62**, 1128–1133.
- 44 S. Sharma, Y. A. Jaimes-Lizcano, R. B. McLay, P. C. Cirino and J. C. Conrad, *Langmuir*, 2016, **32**, 5422–5433.
- 45 R. B. McLay, H. N. Nguyen, Y. A. Jaimes-Lizcano, N. K. Dewangan, S. Alexandrova, D. F. Rodrigues, P. C. Cirino and J. C. Conrad, *Langmuir*, 2018, **34**, 1133–1142.
- 46 S. Wu, *J. Polym. Sci., Part C: Polym. Symp.*, 1971, **34**, 19–30.
- 47 S. Wu, *J. Adhes.*, 1973, **5**, 39–55.

- 48 N. K. Dewangan and J. C. Conrad, *Langmuir*, 2018, **34**, 14012–14021.
- 49 L. Lemelle, J.-F. Palierne, E. Chatre, C. Vaillant and C. Place, *Soft Matter*, 2013, **9**, 9759–9762.
- 50 L. Lemelle, J.-F. Palierne, E. Chatre and C. Place, *J. Bacteriol.*, 2010, **192**, 6307–6308.
- 51 J. Schwarz-Linek, C. Valeriani, A. Cacciuto, M. E. Cates, D. Marenduzzo, A. N. Morozov and W. C. K. Poon, *Proc. Natl. Acad. Sci. U. S. A.*, 2012, **109**, 4052–4057.
- 52 H. Lamb, *Hydrodynamics*, Cambridge University Press, 6th edn, 1945.
- 53 S. Rubinow and J. B. Keller, *J. Fluid Mech.*, 1961, **11**, 447–459.
- 54 Y. Hatwalne, S. Ramaswamy, M. Rao and R. A. Simha, *Phys. Rev. Lett.*, 2004, **92**, 118101.
- 55 A. Baskaran and M. C. Marchetti, *Proc. Natl. Acad. Sci. U. S. A.*, 2009, **106**, 15567–15572.
- 56 G. B. Jeffery, *Proc. Lond. Math. Soc.*, 1915, **14**, 327–338.
- 57 Q. Liu and A. Prosperetti, *J. Fluid Mech.*, 2010, **657**, 1–21.
- 58 N. C. Darnton, L. Turner, S. Rojevsky and H. C. Berg, *J. Bacteriol.*, 2007, **189**, 1756–1764.
- 59 F. T. M. Nguyen and M. D. Graham, *Phys. Rev. E*, 2018, **98**, 042419.
- 60 J. C. Conrad and R. Poling-Skutvik, *Annu. Rev. Chem. Biomol. Eng.*, 2018, **9**, 175–200.
- 61 M. M. Stanton, J. Simmchen, X. Ma, A. Miguel-López and S. Sánchez, *Adv. Mater. Interfaces*, 2016, **3**, 1500505.
- 62 O. Angeles, S. Medina-Moreno, A. Jiménez-González, A. Coreño-Alonso and M. Lizardi-Jiménez, *Chem. Eng. Sci.*, 2017, **165**, 108–112.
- 63 A. Sokolov and I. S. Aranson, *Nat. Commun.*, 2016, **7**, 11114.
- 64 A. Sokolov, L. D. Rubio, J. F. Brady and I. S. Aranson, *Nat. Commun.*, 2018, **9**, 1322.
- 65 C. Krueger, C. Bahr, S. Herminghaus and C. C. Maass, *Eur. Phys. J. E: Soft Matter Biol. Phys.*, 2016, **39**, 64.
- 66 R. Seemann, J.-B. Fleury and C. C. Maass, *Eur. Phys. J.: Spec. Top.*, 2016, **225**, 2227–2240.